Journal of Sports Sciences, 2003, **21**, 75–85

Taylor & Francis
healthsciences

Modelling the flight of a soccer ball in a direct free kick

KEN BRAY and DAVID G. KERWIN*

Department of Sport and Exercise Science, University of Bath, Bath BA2 7AY, UK

Accepted 7 October 2002

This study involved a theoretical and an experimental investigation of the direct free kick in soccer. Our aim was to develop a mathematical model of the ball's flight incorporating aerodynamic lift and drag forces to explore this important 'set-play'. Trajectories derived from the model have been compared with those obtained from detailed video analysis of experimental kicks. Representative values for the drag and lift coefficients have been obtained, together with the implied orientation of the ball's spin axis in flight. The drag coefficient varied from 0.25 to 0.30 and the lift coefficient from 0.23 to 0.29. These values, used with a simple model of a defensive wall, have enabled free kicks to be simulated under realistic conditions, typical of match-play. The results reveal how carefully attackers must engineer the dynamics of a successful kick. For a central free kick some 18.3 m (20 yards) from goal with a conventional wall, and initial speed of 25 $m \cdot s^{-1}$, the ball's initial elevation must be constrained between 16.5° and 17.5° and the ball kicked with almost perfect sidespin.

Keywords: aerodynamics, ball flight, defensive walls, model, soccer.

Introduction

Spin is an important determining factor in the trajectory of a rapidly moving ball. It is usually deliberately applied in the act of kicking, throwing or striking the ball when the player intends to modify the resulting flight. The intention may be to deceive an opponent by swerving a free kick in soccer, pitching a curveball in baseball, or simply to overcome an obstacle in golf by deliberately hooking or slicing the ball around it.

The deflecting force due to the spin of a moving ball is associated with the Magnus effect. The wake of a moving but non-rotating ball is symmetrical about the line of flight, the airflow separating at equivalent points around the ball's surface. With spin, separation occurs earlier at points on the surface advancing into the flow and later for those that are receding. This produces a non-symmetrical wake and a resultant force whose direction is normal to the plane containing the velocity vector and the spin axis of the ball. The deflecting force due to the Magnus effect is frequently referred to as the 'lift' or sometimes the 'sideways' force, although it must be remembered that for some orientations of the spin axis, the force can be downward-pointing. The convention 'lift' to describe the force and the associated aerodynamic constant will be followed in this paper.

* Author to whom all correspondence should be addressed.
e-mail: d.kerwin@bath.ac.uk

General accounts of the physics and mathematics of ball flight are contained in Daish (1972) and de Mestre (1990). Mehta (1985) has also given a comprehensive account of the aerodynamics of sports balls. This latter work is important in emphasizing that not all anomalous aspects of ball flight are derived from Magnus effects alone. Raised seams, such as the pronounced seam on a cricket ball, can also produce non-symmetrical airflow and a differential force that tends to swing the ball in flight.

The first systematic study of spin in a sports context was that of Tait (1896), who showed that backspin would greatly extend the carry of a driven golf ball. Most subsequent work has focused on baseball and golf, where the intention has generally been to determine the lift and drag coefficients so as to interpret the flight characteristics of the ball (see, for example, Davies, 1949; Briggs, 1959; Bearman and Harvey, 1976; Watts and Ferrer, 1987). Alaways and Hubbard (2001) have extended the work for baseballs and have shown that the lift coefficient is significantly affected by the rotating seam, according to whether the ball is pitched in a two-seam or four-seam orientation. This effect is not the same as that seen in seam bowling in cricket, however, where the bowler attempts to deliver the ball with the seam inclined at a fixed angle relative to the line of flight (Mehta, 1985).

The influence of spin on a soccer ball's flight has received little attention by comparison. Fuchs (1991a,b) has produced a detailed theoretical treat-

Journal of Sports Sciences ISSN 0264-0414 print/ISSN 1466-447X online © 2003 Taylor & Francis Ltd
DOI: 10.1080/0264041031000070994

ment of the flight of a spinning ball, but restricts application of the work in soccer to a limited discussion of the trajectory of a corner kick. Lees and Nolan (1998) have further reported that while kicking is the most widely studied football skill – maximal velocity instep kicking in particular – little detailed scientific research has been committed to spin as a determining factor in ball flight in soccer. These authors referred to work by Levendusky *et al.* (1988), who, in a study of impact characteristics of soccer balls, commented on the difficulty of dropping them with repeatable accuracy onto a force plate from a height of 18.1 m. The variability was attributed to 'aerodynamic drag forces and [the] Magnus effect', although no quantitative information was given to support the statement. This lack of committed research on spin effects in soccer is surprising, since the technique is widely used by players in many aspects of the game, especially when trying to beat the defensive wall with a direct free kick.

The defensive wall was introduced very early in the development of the game to counter the threat of a direct shot at goal. Free kicks within the 'D', roughly 18 m from goal, are usually accepted as the most threatening, although elite players continue to stretch this boundary and goals beyond 25 m are not uncommon. Beyond the requirement that defenders must stand 10 yards (9.14 m) from the kick, there are no constraints on the configuration of the wall. Current guidance (Hargreaves, 1990; Hughes, 1999) is that the defenders in the wall should cover the far post of the goal and extend only part of the way to the near post, leaving a clear sight of the kick for the goalkeeper. This arrangement is shown in Fig. 1. It is much frustrated by the practice of members of the attacking side joining the wall to unsight the goalkeeper and breaking away at the instant of the kick.

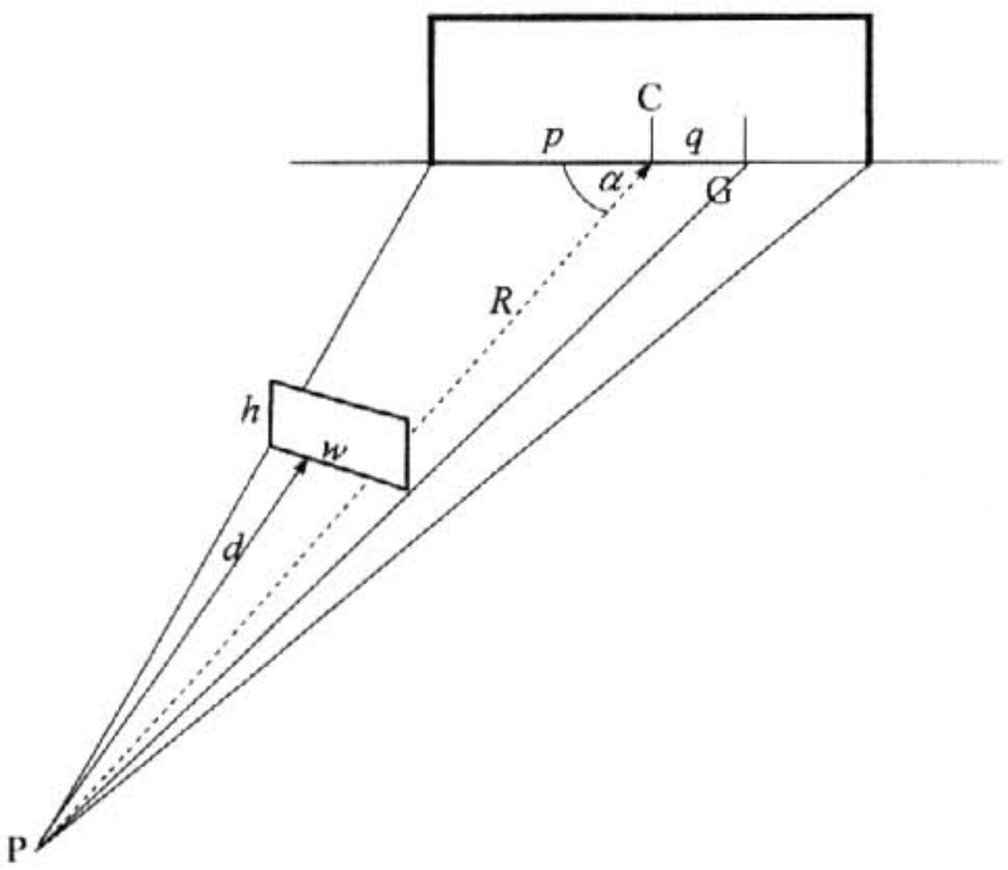

Fig. 1. Geometry of the defensive wall and free kick position. C is the centre of the goal line and G is the goalkeeper's position.

The introduction of the modern ball with its non-absorbent surface may well have accelerated development of the skills necessary for the swerving free kick. Earlier, untreated leather balls were prone to significant water absorption (Armstrong *et al.*, 1988), making the ball less responsive to aerodynamic forces. With the older ball, players would usually shoot very hard at the wall hoping that it would break, leaving a gap, or that the ball would be fortuitously deflected beyond the goalkeeper. Today, coaches and players alike are well aware of the goal-scoring potential of direct free kicks, as elite players are able to swerve the ball over or around the wall in a clean strike at goal. In the 1998 FIFA World Cup, for example, of the 171 goals scored, 42 originated from set-plays, 50% of which were from free kicks (Grant *et al.*, 1999). It is not surprising, therefore, that most teams contain at least one free-kick specialist and that the spectators' expectation of success from a direct free kick is approaching that of the penalty kick.

Here, we describe mathematical models of both the ball's flight in a direct free kick and the associated defensive wall. Our objectives are two-fold: to obtain representative values for the lift and drag coefficients for a soccer ball and to use these in a realistic model of the free kick to determine the constraints the defensive wall places on the kicker in attempting a direct strike at goal.

Methods

Mathematical models

Ball flight

Figure 2 shows the path of a ball, position vector $\boldsymbol{r}$, kicked in the y direction from the origin of a Cartesian frame (x, y, z). At some time t, the velocity vector $\boldsymbol{v}$ is inclined at angle ψ to the (x, y) plane with resolute in this plane at angle θ to the y axis. The unit vector $\boldsymbol{\tau}$ defines the direction of $\boldsymbol{v}$.

Following the impulse of the kick, the ball is assumed to spin about an axis parallel to the (x, z) plane, inclined at constant angle γ to the x axis. This orientation is assumed to remain fixed throughout the flight with no diminution in the spin rate. Under these assumptions, the unit vector $\boldsymbol{\sigma}$, which defines the direction of the spin axis, will have two components, in x and z. This is not unreasonable given the observed action of sidespin

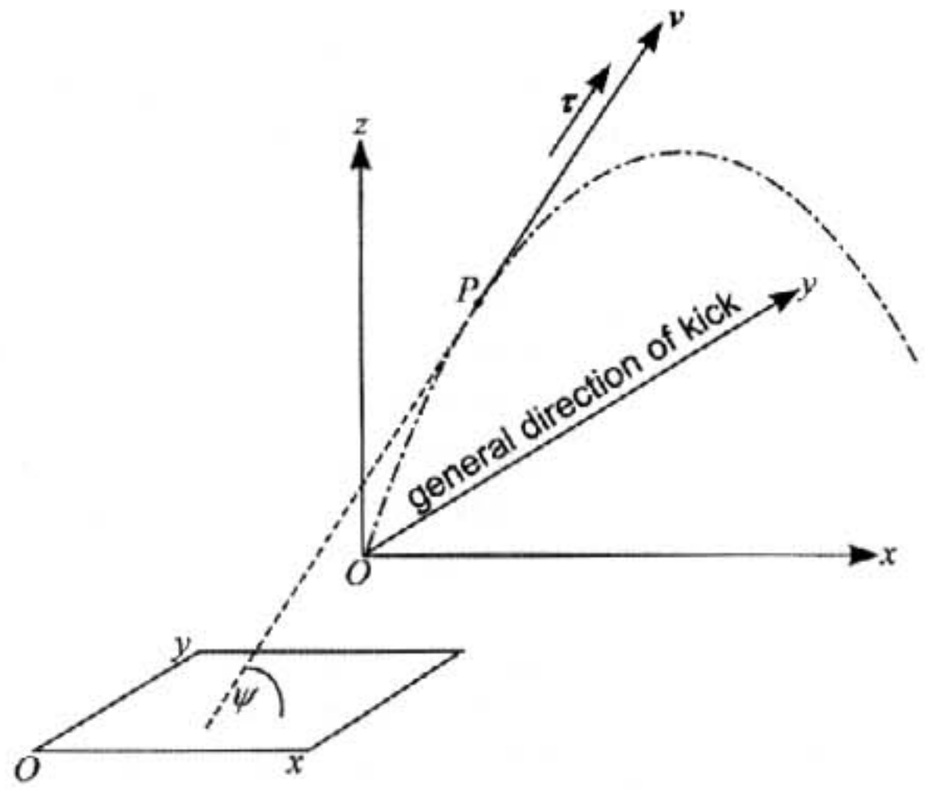

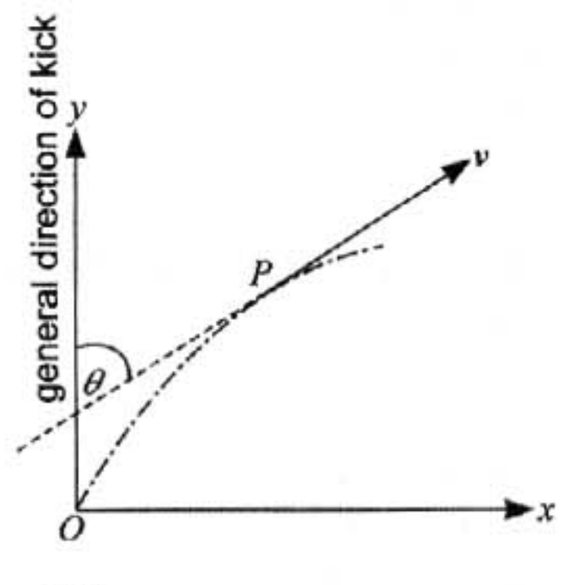

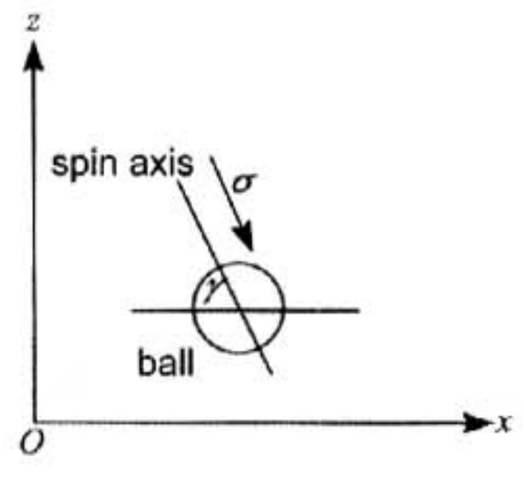

Fig. 2. Definition of coordinate system. The dotted line represents ball trajectory. (a) Velocity vector $\boldsymbol{v}$ inclined at angle ψ to the (x, y) plane. $\boldsymbol{OP} = \boldsymbol{r}(x, y, z)$ is the position vector of the ball. $\boldsymbol{\tau}$ is a unit vector parallel to $\boldsymbol{v}$. (b) Resolute of $\boldsymbol{v}$ in the (x, y) plane inclined at angle θ to the y axis. (c) The spin axis of the ball remains at fixed orientation γ in the (x, z) plane. $\boldsymbol{\sigma}$ is a unit vector parallel to the spin axis.

kicking, where the resulting vertical and lateral deflections are closely dependent on the uprightness achieved in the spin axis at the instant of the kick. A more general treatment of the problem would involve all three components (x, y and z) in $\boldsymbol{\sigma}$, but we have adopted this simpler approach pending more detailed measurement of the spin axis orientation.

Considering only Magnus, drag and gravity forces, and with the subscripts d and l denoting drag and lift respectively, the resultant force $\boldsymbol{F}$ on the ball is

$$\boldsymbol{F} = m\boldsymbol{g} + \boldsymbol{F}_d + \boldsymbol{F}_l$$

where

$$\boldsymbol{F}_d = -\frac{1}{2}\,\rho A v^2 C_d \boldsymbol{\tau} \text{ is the drag force}$$

and

$$\boldsymbol{F}_l = \frac{1}{2}\,\rho A v^2 C_l \boldsymbol{\sigma} \times \boldsymbol{\tau} \text{ is the Magnus (lift) force}$$

In these equations, m is the mass of the ball, A is its cross-sectional area, ρ is the density of air and $v = |\boldsymbol{v}| = \sqrt{(v_x^2 + v_y^2 + v_z^2)}$, where v_x, v_y and v_z are the Cartesian velocity components. C_d and C_l are the drag and lift coefficients.

The differential equation for the flight is, therefore,

$$\ddot{\boldsymbol{r}} = \boldsymbol{g} - k_d v^2 \boldsymbol{\tau} + k_l v^2 \boldsymbol{\sigma} \times \boldsymbol{\tau} \qquad (1)$$

where $\ddot{\boldsymbol{r}} = \mathrm{d}^2\boldsymbol{r}/\mathrm{d}t^2$, $k_d = \rho A C_d/2m$ and $k_l = \rho A C_l/2m$.

From Fig. 2 it can be seen that

$$\boldsymbol{\tau} = \cos\psi\sin\theta\boldsymbol{i} + \cos\psi\cos\theta\boldsymbol{j} + \sin\psi\boldsymbol{k} \quad (2)$$

and

$$\boldsymbol{\sigma} = \cos\gamma\boldsymbol{i} - \sin\gamma\boldsymbol{k} \quad (3)$$

where $\boldsymbol{i}$, $\boldsymbol{j}$ and $\boldsymbol{k}$ are unit vectors on (x, y, z). Furthermore, $v\cos\psi\sin\theta = v_x = \dot{x}$ (i.e. $\cos\psi\sin\theta = \dot{x}/v$). Similarly, $\cos\psi\cos\theta = \dot{y}/v$ and $\sin\psi = \dot{z}/v$.

These expressions can be substituted into equation (2) and the vector product $\boldsymbol{\sigma}\times\boldsymbol{\tau}$ can be evaluated. Substituting the result into equation (1), and collecting the components of $\boldsymbol{i}$, $\boldsymbol{j}$ and $\boldsymbol{k}$, we find that

$$\ddot{x} = -v\{k_d\dot{x} - k_l\sin\gamma\,\dot{y}\} \quad (4)$$

$$\ddot{y} = -v\{k_d\dot{y} + k_l[\cos\gamma\,\dot{z} + \sin\gamma\,\dot{x}]\} \quad (5)$$

$$\ddot{z} = -g - v\{k_d\dot{z} - k_l\cos\gamma\,\dot{y}\} \quad (6)$$

These equations have no closed form solutions but can be solved numerically using a Runge-Kutta routine, for example, given the initial conditions for γ, x, $\dot{x}$, etc., and the constants m, A and ρ. The parameters C_d and C_l present problems, however, in view of the lack of quantitative information for soccer balls. A value of $C_d = 0.2$ has been suggested by de Mestre (1990), with C_l determinable from experimental data for a smooth sphere, after Davies (1949). The assumption of 'smoothness' for a soccer ball is questionable and our approach has been to compare the model predictions with a controlled series of experimental kicks. Details of how C_d and C_l have been obtained from this procedure are given in the 'Data analysis' section. A fundamental assumption is that C_d and C_l remain constant in equations (4)–(6). This is the case provided post-critical Reynolds numbers prevail throughout the flight and this is addressed for the measured trajectories under 'Experimental findings'.

Defensive wall

The assumed position of the wall relative to the kick is shown in Fig. 1. With the geometry of the figure it can be shown that

$$w = d\sin\alpha[p/(R - p\cos\alpha) + q/(R + q\cos\alpha)] \quad (7)$$

Here, $2p$ is the width of the goal, w is the required width of the wall, d is the compulsory 10 yard (9.14 m) distance and R and α are the distance and angle of the free kick, respectively. The parameter q represents the implied coverage of the goal line by the wall, ranging from complete cover ($q = p$) to a portion of the line left open for the goalkeeper's view of the shot ($0 < q < p$). There are no explicit recommendations for this parameter in practice (Hargreaves, 1990; Hughes, 1999) and so $q = p/2$ has been chosen as a reasonable compromise. The number of defenders in the wall for various distances and angles can be calculated from equation (7) by dividing w by the average player's width. This number is of interest in practical coaching but not explicitly required in the analysis that follows.

The wall height (h) has not so far been considered, but can be taken as the average player height. The wall, therefore, is modelled by a rectangle of dimensions $w \times h$ and can be used in conjunction with solutions of equations (4)–(6) to determine the constraints the defensive wall imposes on a free kick from some defined position.

Determination of aerodynamic parameters C_d and C_l

Free kick trials

A male player who had provided written informed consent performed a series of trial kicks. He was skilled in striking a ball with spin and launch velocity representative of a realistic free kick. A large indoor sports hall was used for the trials to ensure that the ball's flight could be monitored in still air, free from any external disturbances. Other than requiring the player to simulate the action of a free kick some 20 yards (18.3 m) from goal, with an imagined wall of the regulation height and distance, no special constraints were imposed. We monitored a series of 10 sidespin kicks, for which the player was asked to strike the ball from the ground with as nearly a vertical spin axis as possible. Sidespin is the most commonly used technique by elite players in seeking to swerve a ball beyond the goalkeeper's reach. Our player was left-footed and with conventional instep kicking would be expected to spin the ball clockwise when viewed from above and to swerve it from left to right.

Experimental design and data capture

Two digital video camcorders (Sony CCD-TRV900E, Japan) were located at the corners of the sports hall (Fig. 3) approximately 32 m apart, 1.50 m above the ground and at a distance of 33 m from the centre of the line of intended ball flight. Video recordings were made while a single pole (height 3.20 m, containing

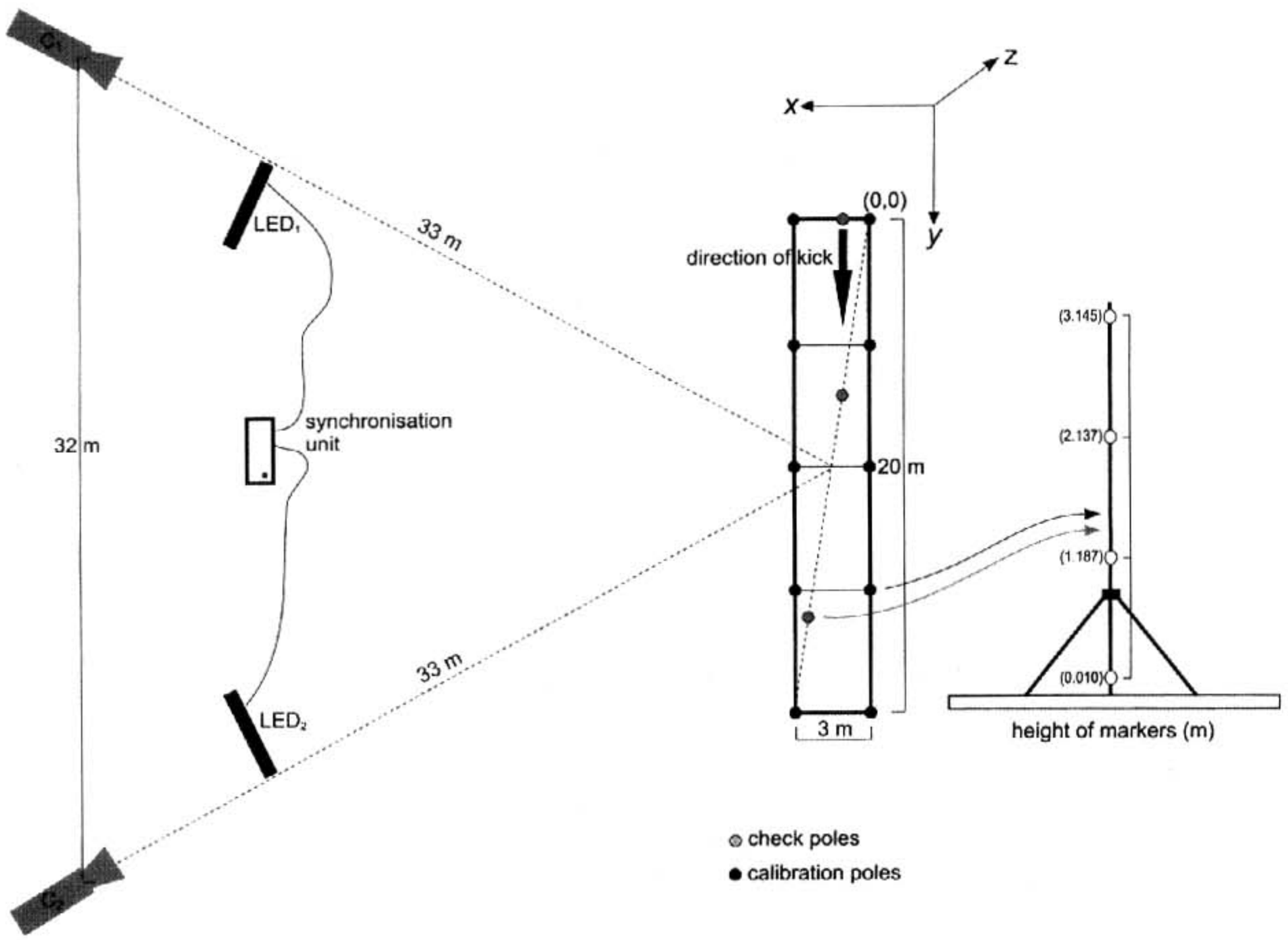

Fig. 3. Camera, LED synchronization unit and calibration pole positions in the sports hall for kicking trial data collection.

four 0.10 m diameter spherical markers located at heights of 0.101, 1.187, 2.137 and 3.145 m) was moved in sequence around 10 carefully measured locations encompassing a volume of $20 \times 3 \times 3.145$ m. Recordings were also made with the calibration pole located at the initial ball position and at two points along a diagonal in the (x, y) plane at 7 and 16 m from the origin to enable positional accuracy within the calibrated volume to be determined independently.

Each camera was operated at 50 Hz with shutter exposure times of 1/1000 s. The focal length of the lens on each camera was adjusted until the whole of the calibrated volume was within the field of view. Each camera's pan, tilt and roll angles and the focal length of the lens were locked throughout the data collection. Dates and times were recorded onto each tape, enabling the corresponding video sequences to be paired. A synchronization unit, as used by Kerwin and Trewartha (2000), comprising 20 light-emitting diodes (LEDs) was placed between each camera and the calibrated volume. A radio-controlled trigger simultaneously initiated the illumination of 20 LEDs at 1 ms intervals for each kicking trial. All digitizing was completed by the same skilled operator using the 'Target' system (Kerwin, 1995). The four spherical markers in 10 calibration and three checking locations were digitized six times. The position of the ball in each of the kicking sequences was digitized from when the ball was clearly in free flight (approximately 0.1 s after initial foot contact) to when the ball passed out of the calibration volume. Camera calibration was carried out using a 12-parameter direct linear transformation (DLT) procedure (Karara, 1980). The three-dimensional coordinates of the ball location were reconstructed by finding a least-squares solution to four planes defined by the DLT equations. An estimate of the reconstruction error was calculated as an unbiased root mean square distance from the four planes.

Synchronization of each pair of digitized data was determined using the time offset in milliseconds between the video images containing the initial LED displays. An interpolating quintic spline (Wood and Jennings, 1979) was used to generate matching data points for the time-shifted data set.

Data analysis

The experimental results for each of the kicks were analysed in the following way. Positional information for the ball was stored in individual data arrays for x, y and z as functions of time, t, in seconds. Polynomials were fitted to the positional data for x, y and z in the form

$$x = a_0 + a_1 t + a_2 t^2 + a_3 t^3 + a_4 t^4 \qquad (8)$$

The coefficients a_0 to a_4 were determined from the Levenberg-Marquardt algorithm (Press *et al.*, 1992). The velocity components v_x, v_y and v_z were then obtained by numerical differentiation of these new positional data. The initial values for x, v_x, etc., to be used in the Runge-Kutta solutions of equations (4)–(6) were obtained from the new positional and velocity data arrays at $t = 0.1$ s. Visual inspection of the raw data indicated that an elapsed time of 0.9 s was sufficient to cover a 20 m flight, adequate for representing a realistic kick.

The parameters γ, C_d and C_l were determined for each kick as follows. Initial values were chosen and the differential equations solved to produce the appropriate predicted trajectory. A parameter ε was determined for the complete trajectory by examining the root mean square error in the quantity $\boldsymbol{r}_p - \boldsymbol{r}_m$, where $\boldsymbol{r}_p$ and $\boldsymbol{r}_m$ represent the position vectors of the model (predicted) and experimental (measured) data. Iterations were repeated until a minimum value of ε was obtained. The process was found to be stable and convergent with an average value of $\varepsilon = 0.052$ m for the 10 kicks.

Results and discussion

Error analysis

Reconstruction errors

Reconstruction errors from the DLT analysis based on six repeat digitizations of four markers on the calibration pole in 10 locations were 0.011, 0.007 and 0.005 m in the x, y and z directions, respectively, with a resulting overall root mean square error of 0.008 m.

Digitizing errors

The accuracy with which well-defined stationary points could be located within the calibrated volume was determined by comparing the known locations of the four spheres mounted on the moveable pole at three positions within the calibration volume (Fig. 3). Six repeat digitizations of the 12 known locations resulted in root mean square errors in x, y and z of 0.021, 0.015 and 0.007 m, respectively, with an overall root mean square error of 0.026 m.

Table 1. Summary of experimental results (v_i and v_f are the velocities at 0.1 s and 0.9 s, respectively)

Velocity ($\mathrm{m \cdot s^{-1}}$)		Spin angle $\gamma(^\circ)$	C_d	C_l
v_i	v_f	± 4	± 0.03	± 0.05
23.0	17.9	71	0.27	0.29
26.3	19.8	95	0.29	0.29
26.8	20.1	96	0.30	0.28
24.8	19.6	83	0.25	0.23
24.2	19.1	71	0.28	0.27
25.7	18.4	66	0.28	0.25
25.1	19.4	77	0.27	0.29
24.9	18.6	61	0.28	0.23
24.4	19.1	83	0.28	0.24
28.3	20.4	80	0.27	0.26

Implicit errors in γ, C_d and C_l

The differential equations (4)–(6) do not yield closed form solutions containing γ, C_d and C_l explicitly and so it was not possible to undertake a conventional error analysis for these quantities. A simulation approach was used instead. For each kick, the x, y and z values obtained from the polynomials defined by equation (8) were compared with the raw data values for each point on the trajectory. This enabled the standard deviations in the experimental coordinates to be determined using the fitted polynomial values as the basis. Averaged over all 10 kicks, the standard deviations were found to be:

$$s_x = 0.017 \text{ m}$$
$$s_y = 0.008 \text{ m}$$
$$s_z = 0.010 \text{ m}$$

It was then possible to define a modified experimental trajectory by perturbing the measured coordinates using a random normal deviate (rnd) in the form

$$x \rightarrow x \pm \mathrm{rnd}(1.96 \cdot s_x)$$

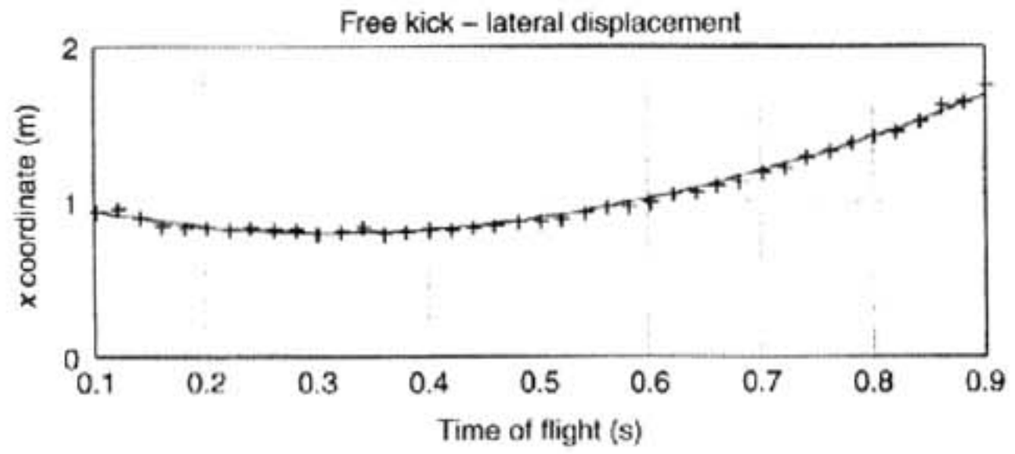

Fig. 4. Comparison of predicted and measured trajectories.

with similar expressions for y and z. New values of γ, C_d and C_l were then obtained for the modified experimental trajectory by re-solving the differential equations (4)–(6). From 50 replications of this process, the implicit errors in the quantities were estimated to be $\gamma \pm 4°$, $C_d \pm 0.03$ and $C_l \pm 0.05$.

Experimental findings

Table 1 summarizes the results and includes the initial and final ball speeds for each kick. The lowest speed recorded, 17.9 $m \cdot s^{-1}$, gives a Reynolds number (Re) of 2.5×10^5. Transition to post-critical conditions is usually taken to occur at Re $> 2.1 \times 10^5$, and so post-critical conditions can be assumed for all of our measured trajectories.

The values of C_d exceed those generally quoted of around 0.2 for soccer balls (Daish, 1972; de Mestre, 1990), although, as already noted, there is little published information on experimental values in this area. As we were unable to obtain the spin rate explicitly, no general conclusions can be drawn about the C_l values in Table 1. All that can be said is that the parameters are more representative of 'rough' spheres within the range of conditions prevailing in soccer (cf. Bearman and Harvey, 1976), although more work is needed to corroborate this.

Figure 4 shows comparisons between a measured and predicted trajectory for one of the kicks in our series where the parameters were determined to be $\gamma = 83°$, $C_d = 0.25$ and $C_l = 0.23$. Agreement between the measured and predicted trajectory for the individual coordinates is good (a root mean square error of $\varepsilon = 0.045$ m was obtained for this case). Figure 4 also gives some indication of the amount of swerve that can be imparted to the ball in practice. Sidespin can easily be achieved with conventional instep kicking and very nearly pure sidespin ($\gamma = 83°$) was produced by our player in this case.

Simulated free kicks with defensive wall

To assess the constraints imposed on the kicker by the defensive wall, representative values from the trials of $C_d = 0.28$ and $C_l = 0.26$ were chosen. Taking $\alpha = 90°$ and $R = 20$ yards (18.28 m) in Fig. 1 would represent a central free kick symmetrically within the 'D'. A defensive wall of height 1.83 m with geometry defined by equation (7) is assumed. The goalkeeper (G) is assumed to take the position indicated in Fig. 1, with the wall blocking 75% of the goal line ($q = 1.83$ m). Figure 5 shows a scale diagram of the free kick position with respect to the pitch markings.

Although it would be possible to analyse this position exhaustively using various angles, distances and widths of the wall, the main features can be revealed by taking some illustrative values of the parameters. Sidespin kicks with a right-footed kicker will be assumed, taking an initial kicking speed of 25 $m \cdot s^{-1}$. While the ball could be swerved around the wall below the height of the defenders, most attackers choose to play the ball over the wall, towards the far post and beyond the goalkeeper's reach. This has the added advantage of obscuring the ball during the early portion of its flight, further reducing the goalkeeper's reaction time.

Figure 6a shows the path of a ball kicked at a speed of 25 $m \cdot s^{-1}$ with an elevation of 16.5°. Pure sidespin ($\gamma = 90°$) has been assumed. The initial direction of the kick is taken to be down the centre line to goal. This ball would just clear the wall and would cross the goal line, under the bar, approximately 4 m from the goalkeeper's position. Kicking at an inclination of 3.5° to the centre line, towards the far post, with the same initial conditions, would result in the ball entering the net just inside the far post.

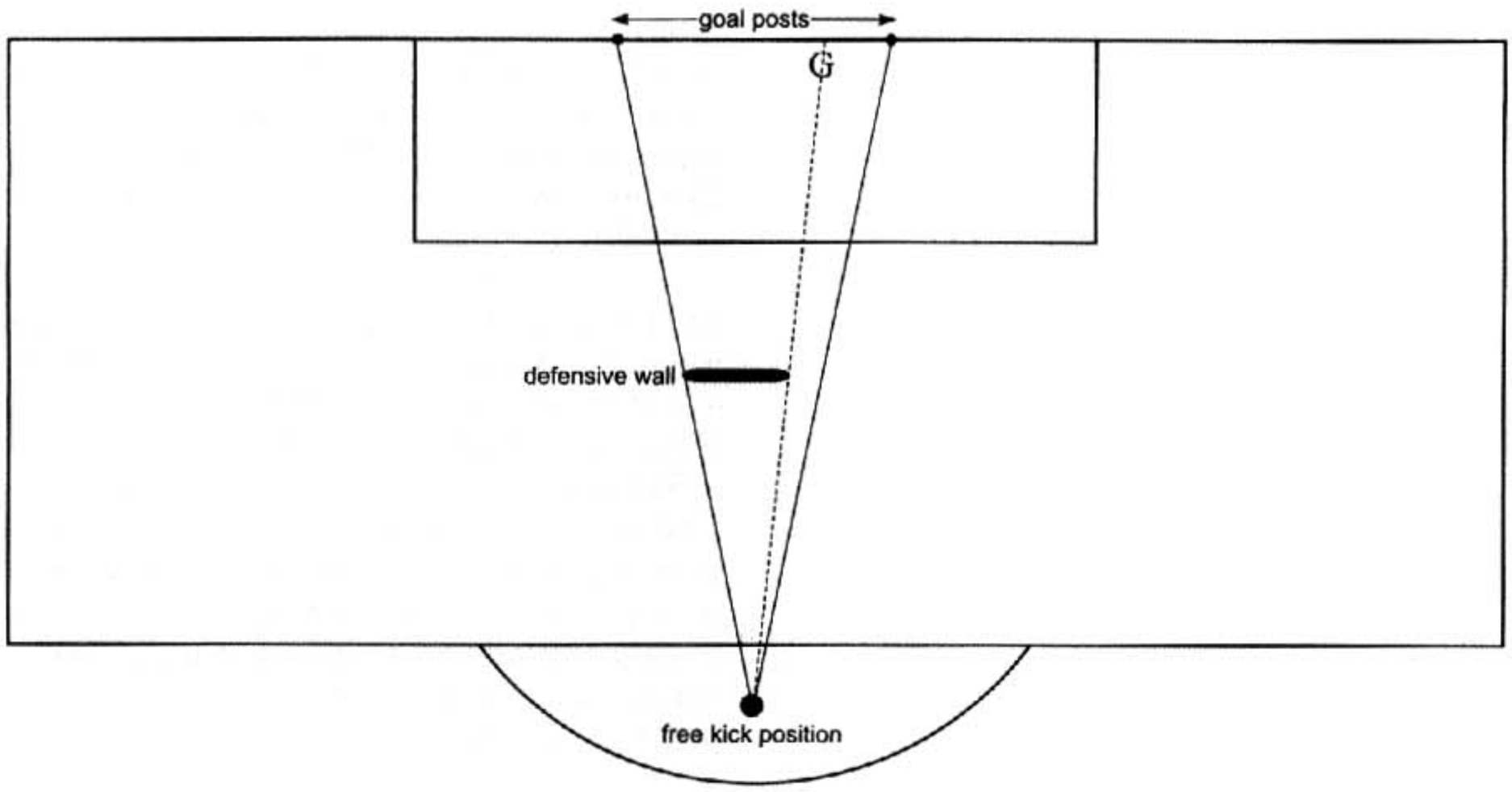

Fig. 5. The free kick and defensive wall positions used in the kick simulations.

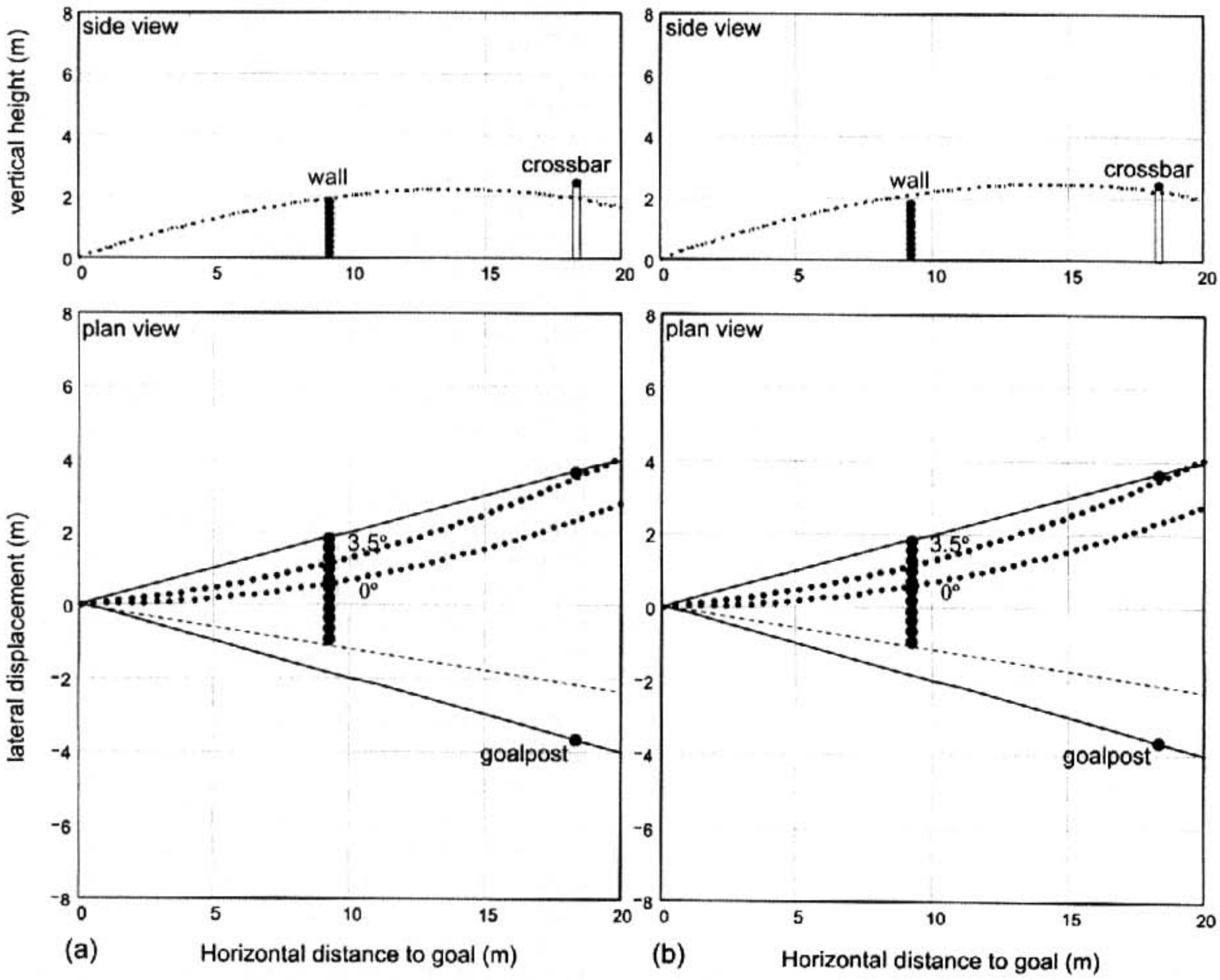

Fig. 6. Simulated free kick. (a) Ball speed 25 $m \cdot s^{-1}$, initial elevation 16.5°, spin axis 90° to horizontal. Initial kicking directions 0° and 3.5° to centre line to goal. (b) Ball speed 25 $m \cdot s^{-1}$, initial elevation 17.5°, spin axis 90° to horizontal. Initial kicking directions 0° and 3.5° to centre line to goal.

Figure 6b differs from Fig. 6a only in the assumption of the initial elevation of the kick. If this were increased by as little as 1° to 17.5°, the ball would clear the wall but would only just pass under the bar for both directions of kick.

Similar constraints apply to the initial velocity of the kick. As Fig. 7a shows, a ball kicked with an initial elevation of 16.5° but with an initial velocity of 26 $m \cdot s^{-1}$ would only just pass under the bar. Control of the orientation of the spin axis is also important. Figure 7b represents an initial elevation of 16.5° and a kicking speed of 25 $m \cdot s^{-1}$, but with the spin axis reduced by 7° from the vertical to 83°. The outcome is virtually identical to that in Fig. 7a, with the backspin introduced by tilting the spin axis slightly being as detrimental to the kick as increased kicking velocity.

The above results illustrate how closely the striker must control the parameters of the kick to achieve a successful outcome. By the same token, little can be done by the goalkeeper in attempting a save when the ball is struck correctly. A further constraint is placed on the goalkeeper if the ball is not seen at the instant it is played, but only when it first clears the defensive wall. The time of flight to goal from this point, using the parameters in the above examples, would typically be 0.45 s, leaving virtually no margin for indecision, even for a shot with very little swerve.

Conclusions

The objectives of this study were to obtain representative values for the drag and lift coefficients for soccer balls and to use these in a realistic model of a free kick with associated defensive wall. Video analysis of ball flight for a series of free kicks enabled successive ball positions to be accurately determined and hence

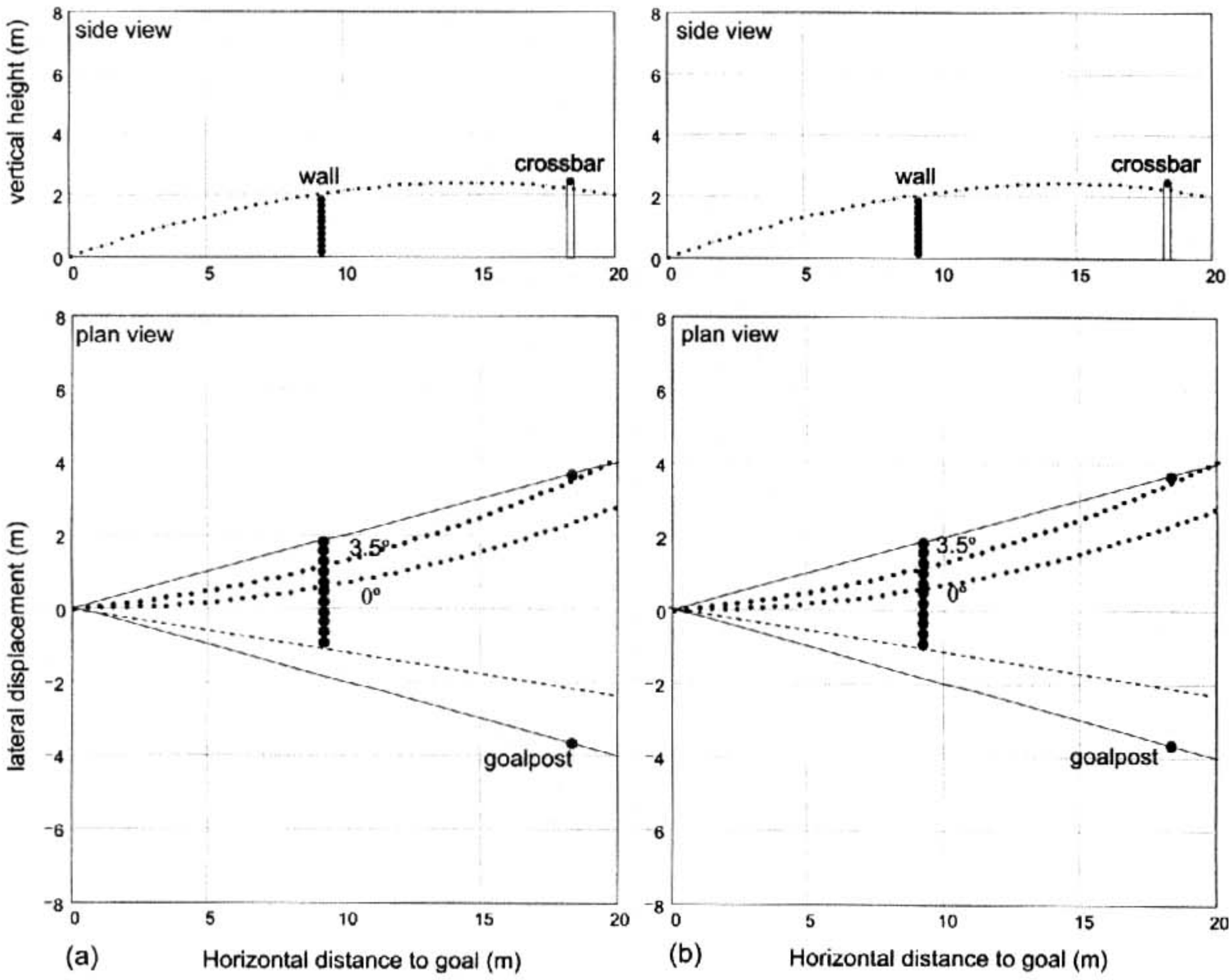

Fig. 7. Simulated free kick. (a) Ball speed 26 $m \cdot s^{-1}$, initial elevation 16.5°, spin axis 90° to horizontal. Initial kicking directions 0° and 3.5° to centre line to goal. (b) Ball speed 25 $m \cdot s^{-1}$, initial elevation 16.5°, spin axis 83° to horizontal. Initial kicking directions 0° and 3.5° to centre line to goal.

facilitated the estimation of the required aerodynamics parameters. Lack of published experimental data for soccer balls has not enabled us to compare our findings with data derived from wind tunnel tests, for example. The values determined do, however, produce deflections, which, when used in conjunction with other parameters typical of free kicks in soccer, are in line with those observed in match-play. This lends confidence to use of the flight model, in conjunction with a simple model of the defensive wall, to explore the constraints posed by the wall in a direct free kick. A particular style of free kick has been used to illustrate the models, but this could readily be extended by variation of a few parameters to more complex geometries and to a systematic study of the optimal strategies for attackers and defenders in this important set-play.

We have restricted the present study to the sidespin free kick, although there is ample evidence that elite players are able to strike a ball from the ground with topspin, producing a free kick that descends (dips) much more rapidly than its sidespin counterpart. The more rapid descent is associated with the downward-pointing component of the Magnus force for this case. With this type of kick, the ball can be struck relatively harder with a corresponding increase in velocity and a reduction in the flight time to goal. Examination of Table 1 reveals that our player achieved a small component of topspin in two kicks where the orientation of the spin axis exceeded 90°. This type of kick, although more demanding in terms of the precision with which the ball must be struck, can be very easily modelled with appropriate adjustment of the terms in the differential equations for the flight and is the subject of ongoing work.

As noted, we have to date been unable to determine spin rate for the ball explicitly and have represented this quantity implicitly via the lift coefficient, C_l, in the equations of motion. Work in progress will enable spin rate to be measured at the instant of the kick, together with the implied orientation of the ball's spin axis, as both affect the resultant trajectory significantly.

Acknowledgements

We gratefully acknowledge the Department of Sports Development, University of Bath, who provided the university sports hall for our experimental work. Thanks also to Andreas Wallbaum, Greg Sharp and Paul Bullock for assistance with the data collection.

References

Alaways, L.W. and Hubbard, M. (2001). Experimental determination of baseball spin and lift. *Journal of Sports Sciences*, **19**, 349–358.

Armstrong, C.W., Levendusky, T.A., Spryropoulous, P. and Kugler, L. (1988). Influence of inflation pressure and ball wetness on the impact characteristics of two types of soccer balls. In *Science and Football* (edited by T. Reilly, A. Lees, K. Davids and W.J. Murphy), pp. 394–398. London: E & FN Spon.

Bearman, P.W. and Harvey, J.K. (1976). Golf ball aerodynamics. *Aeronautical Quarterly*, **27**, 112–122.

Briggs, L.J. (1959). Effect of spin and speed on the lateral deflection (curve) of a baseball; and the Magnus effect for smooth spheres. *American Journal of Physics*, **27**, 589–596.

Daish, C.B. (1972). *The Physics of Ball Games*. London: English Universities Press.

Davies, J.M. (1949). The aerodynamics of golf balls. *Journal of Applied Physics*, **20**, 821–828.

de Mestre, N. (1990). *The Mathematics of Projectiles in Sport*. Cambridge: Cambridge University Press.

Fuchs, P.M. (1991a). Physical model. Theoretical aspects and applications of the flight of a ball in the atmosphere. Part I: Modelling of forces and torque, and theoretical prospects. *Mathematical Methods in the Applied Sciences*, **14**, 447–460.

Fuchs, P.M. (1991b). Physical model. Theoretical aspects and applications of the flight of a ball in the atmosphere. Part II: Theoretical aspects in the case of vertical angular frequency and applications. *Mathematical Methods in the Applied Sciences*, **14**, 461–481.

Grant, A.G., Williams, A.M. and Reilly, T. (1999). Analysis of goals scored in the 1998 World Cup. *Journal of Sports Sciences*, **17**, 826–827.

Hargreaves, A. (1990). *Skills and Strategies for Coaching Soccer*. Champaign, IL: Leisure Press.

Hughes, C. (1999). *The F.A. Coaching Book of Soccer Tactics and Skills*. Harpenden: Queen Anne Press.

Karara, H.M. (1980). Non-metric cameras. In *Developments in Close Range Photogrammetry*, Vol. 1 (edited by K.B. Atkinson), pp. 63–68. London: Applied Science.

Kerwin, D.G. (1995). Apex/Target high resolution video digitising system. In *Proceedings of the Biomechanics Section of the British Association of Sport and Exercise Sciences* (edited by J. Watkins), pp. 1–4. Glasgow: BASES.

Kerwin, D.G. and Trewartha, G. (2000). Strategies for maintaining a handstand in the anterior-posterior direction. *Medicine and Science in Sports and Exercise*, **33**, 1182–1188.

Lees, A. and Nolan, L. (1998). The biomechanics of soccer: a review. *Journal of Sports Sciences*, **16**, 211–234.

Levendusky, T.A., Armstrong, C.W., Eck, J.S., Spryropoulous, P., Jeziorowski, J. and Kugler, L. (1988). Impact characteristics of two types of soccer balls. In *Science and Football* (edited by T. Reilly, A. Lees, K. Davids and W.J. Murphy), pp. 385–393. London: E & FN Spon.

Mehta, R.D. (1985). Aerodynamics of sports balls. *Annual Review of Fluid Mechanics*, **17**, 151–189.

Press, W.H., Flannery, W.T., Teukolsky, S.A. and Vetterling, B.P. (1992). *Numerical Recipes in C.* New York: Cambridge University Press.

Tait, P.G. (1896). On the path of a rotating spherical projectile. *Transactions of the Royal Society, Edinburgh*, **16**(part 2), 491–506.

Watts, R.G. and Ferrer, R. (1987). The lateral force on a spinning sphere. *American Journal of Physics*, **55**, 40–45.

Wood, G.A. and Jennings, L.S. (1979). On the use of spline functions for data smoothing. *Journal of Biomechanics*, **12**, 477–479.